On the significance of interparticle friction to the mechanical behaviour of clay

Yohei Nakamichi [1*], *Catherine* O'Sullivan [2], *Paul* Tangney [3,4], and *Stefano* Angioletti-Uberti [4]

[1] Geotechnical Engineering Department, Technology Research Institute, Technology Division, Obayashi Corporation, Tokyo, Japan
[2] Department of Civil and Environmental Engineering, Imperial College London, London, UK
[3] Department of Physics, Imperial College London, London, UK
[4] Department of Materials, Imperial College London, London, UK

Abstract. This study investigates the influence of interparticle friction on the one-dimensional (1D) compression behaviour of normally consolidated clay using coarse-grained molecular dynamics (CGMD). CGMD is a particle-scale simulation method where individual clay particles are modelled as flat ellipsoids, and the interactions between particles are described by considering the potential energy of the interaction. This potential energy depends on the distance between clay platelets. In the case of kaolinite DLVO theory can be used to predict this energy. Most potential energy functions that have been used in particle-scale simulations do not explicitly include interparticle friction, and so their predictions of key geotechnical behaviour are unreliable. This study uses a potential energy function that models interparticle tangential forces with a spring-slider (Coulomb) friction model. 1D compression simulations were then conducted on virtual samples of kaolinite assuming pore water pH values of 4 and 8, giving flocculated and dispersed microfabrics, respectively. We show that if interparticle friction is omitted in 1D compression simulations the resulting lateral earth pressure coefficients are unrealistic (i.e. K_0=1.0), and that including friction gives more physically accurate K_0 values (i.e. K_0 <1.0). Unloading-reloading simulations revealed that interparticle friction is essential to reproduce the hysteretic behaviour which can be experimentally observed in consolidation tests. These findings underscore the importance of incorporating interparticle friction in particle-scale simulations of clay and highlight the need to better understand friction on clay particle surfaces in geomechanics.

1 Introduction

Coarse-grained molecular dynamics (CGMD), in which the elementary particles are clay platelets and they are modelled as flat rigid ellipsoids, has been introduced as a particle-scale simulation method in geotechnical engineering [1]. While CGMD is algorithmically similar to the discrete-element method (DEM), interactions between clay platelets are described considering the potential energy (U) of the interaction, not physical contact force between clay platelets. In CGMD this potential energy is modelled using potential functions which calculate U as the function of the distance between clay platelets (h). The potential functions need to be calibrated against the U- h relationships obtained theoretically or via atomic-scale simulation. In the case of kaolinite Derjaguin-Landau-Verwey-Overbeek (DLVO) theory [2,3] is widely used to calibrate them.

DLVO theory considers only the non-contact components of interactions such as the van der Waals and the electrostatic interactions, hence the role of interparticle friction (tangential contact force) is less obvious in an implementation of the CGMD framework of kaolinite. DEM simulation data of sand have indicated that interparticle friction significantly contributes to the overall mechanical response [4,5,6]. Bandera et al. [7] investigated the impact of the coefficient of friction (μ) on the lateral earth pressure coefficient (K_0) via DEM one-dimensional (1D) compression simulations using sphere particles and showed that the K_0 value decreases as the μ value increases. Furthermore, Bandera et al. [7] indicated that the absence of interparticle friction in CGMD simulations of kaolinite results in the isotropic stress tensor despite the anisotropic particle arrangement generated. This result obviously conflicts with the mechanical behaviour of clay obtained in laboratory tests. With reference to these available DEM and CGMD simulation data, interparticle friction must be explicitly included in CGMD framework to capture key geotechnical behaviour of clay.

This study focuses on the need to incorporate interparticle friction in CGMD simulations of kaolinite and its influence on behaviour in 1D compression. This study used a potential function which computes interparticle tangential forces (friction) with a spring-slider (Coulomb) friction model. 1D compression simulations were then conducted on virtual kaolinite samples.

* Corresponding author: nakamichi.yohei@obayashi.co.jp

2 Methodology

2.1 Modelling of kaolinite particle

In the CGMD framework used in this study, clay platelets were modelled as flat and rigid ellipsoidal particles with a diameter of 2.0 μm and a thickness of 0.2 μm, as shown in Fig. 1, simulating kaolinite particles. Each ellipsoidal particle was divided into three domains corresponding to the alumina face (Af), the silica face (Si), and the edge (E) surfaces of kaolinite particles. This segmentation of ellipsoidal particles was necessary to capture different interaction energies between the six possible relative particle orientations of pairs of ellipsoidal particles, i.e. Af-Af, Af-Si, Si-Si, Af-E, Si-E, and E-E.

2.2 Calculation of potential energy

The potential energy between two ellipsoidal particles is calculated using potential functions that gives $\boldsymbol{U}$ as a function of $\boldsymbol{h}$ and the relative particle orientations. The corresponding interaction force vector ($\mathbf{F}$) is given by the negative gradient of $\boldsymbol{U}$ with the centre-to-centre vector ($\mathbf{r}$) between two ellipsoidal particles (i.e. $\mathbf{F} = -\partial \boldsymbol{U}/\partial \mathbf{r}$). This study used the potential function developed by Nakamichi et al. [8,9,10], which was built upon the Gay-Berne potential function [11] that is a general version of the Lennard Jones potential for ellipsoidal particles. This potential function has three terms, namely a long- and middle-range repulsion, a short-range attraction, and a very short-range repulsion, corresponding to the electrostatic energy, the van der Waals energy, and the Born repulsion. This potential function can simulate non-linear and non-monotonic nature of the $\boldsymbol{U}$- $\boldsymbol{h}$ relationships predicted by DLVO theory and has positive and negative local maxima in the interaction energy (termed an energy barrier and an energy well, respectively). The energy barrier and the energy well play significant role of the mechanical response of clay [9]. The specific equation and the detailed calibration procedure of the potential function using DLVO theory are described in Nakamichi et al. [8,9].

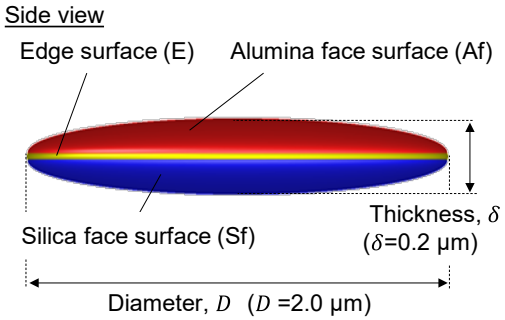

Fig.1. Kaolinite particle model (rigid flat ellipsoid) adopted in the coarse-grained molecular dynamics simulations.

2.3 Assumption of pore water conditions

The surface charge of kaolinite particles is highly dependent on pore water pH, resulting in a variation in the U- h relationships [12,13]. This study assumed two pore water conditions, pH values of 4 and 8. Fig.2 shows the representative U- h relationships for each pH value predicted using DLVO theory. At pH=8 (alkaline pore water), all interactions are repulsive, i.e. they include an energy barrier. On the other hand, at pH=4 (acidic pore water), some interactions are repulsive whereas other interactions are always attractive because of the heterogeneity of the surface charge at pH=4 [14]. These attractive interactions do not have an energy barrier.

The differences in the U- h relationships result in clay different microfabrics. Scanning electron microscope (SEM) images have shown that a kaolinite sample saturated with a pH=4 pore water has a flocculated microfabric and that saturated with a pH=8 pore water has a dispersed microfabric, respectively [15].

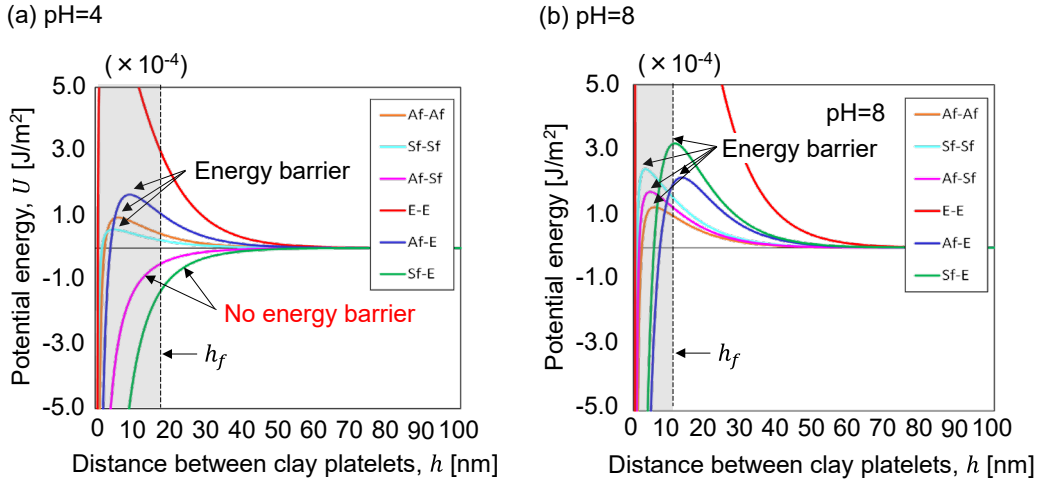

Fig. 2. Variation in potential energy with distance of clay platelets for kaolinite particles saturated with (a) pH4 pore water and (b) pH8 pore water predicted by DLVO theory (E - edge, Af - alumina face, Sf - silica face, Af-Af indicates alumina face interacting with alumina face, E-E indicates edge interacting with edge, etc.).

2.4 Consideration of interparticle friction

Interparticle friction is a resistance encountered when two particles in contact move relative to each other, and its force acts in a direction that opposes the relative sliding motion of their contact surface, i.e. parallel to the contact surface. Unlike interaction forces such as the electrostatic and the van der Waals forces, the interparticle friction forces do not comply with the energy conservation law.

Most of the previous particle-scale simulations of clay using DEM and CGMD have employed a Coulomb friction model to describe the interparticle frictions. The Coulomb friction model calculates the interparticle friction (tangential) forces using a virtual spring and slider. When two particles are sticking (not sliding), the interparticle friction force is proportional to the cumulative tangential displacement determined by the contact history. When two particles are sliding, i.e. the magnitude of the interparticle friction force reaches the value obtained by multiplying the magnitude of the normal force by the coefficient of friction (μ), the interparticle friction force is controlled not to increase further. Additionally, these previous particle-scale simulations of clay did not explicitly consider cohesion for simplicity, yet there were able to reproduce fundamental mechanical behaviour of clay.

However, a consensus of what is the best way to describe interparticle friction of clay analytically or numerically and which friction model should be adopted has not been reached because the origin of friction remains unresolved. Hence, future studies should address it.

This study used a new framework that includes a Coulomb friction model and introduced interparticle friction cut-off length (h_f). The position of h_f on the U-h relationship is shown in Fig. 2. Interparticle friction is activated when $h \leq h_f$, while it is inactive when $h > h_f$. The detailed implementation of the Coulomb friction model with h_f in the CGMD framework is explained in Nakamichi et al. [10].

3 1D compression simulations

3.1 Virtual samples and simulation process

Two virtual kaolinite samples with different assumed pore water pH values, pH=4 (acidic) and pH=8 (alkaline), were prepared. At first, particles were evenly spaced at 2.05 μm in intervals in a cubic simulation box with a length of 45.1 μm. The number of particles in the simulation box was 10,648 (arranged in $22 \times 22 \times 22$ grid). To reproduce a bulk behaviour, periodic boundary conditions were applied in all directions (x, y, and z). In the initial state, each particle was assigned a random orientation, hence the distribution of particle orientations was isotropic. Each particle was given an initial velocity based on a Gaussian distribution so that the kinetic energy of the samples corresponded to 300 K.

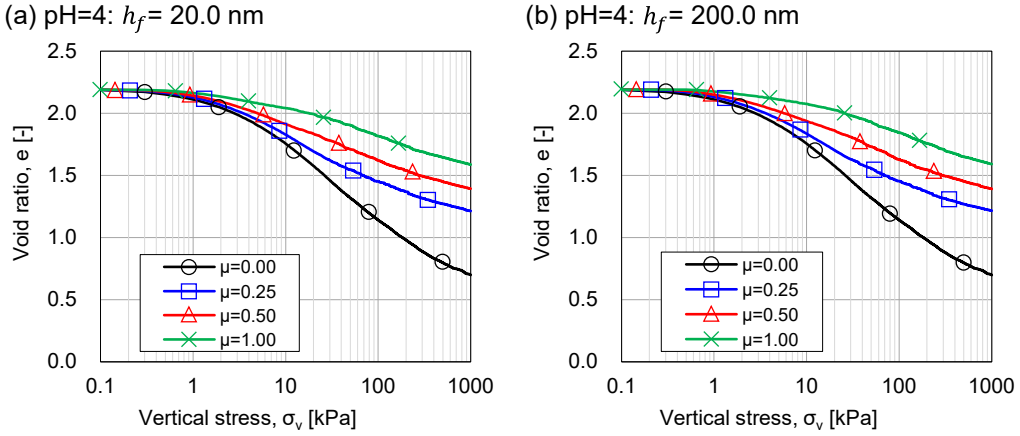

Fig. 3. e-log(σ_v') relationships for pH=4 samples with different values of μ: (a) $h_f = 20$ nm, and (b) $h_f = 200$ nm.

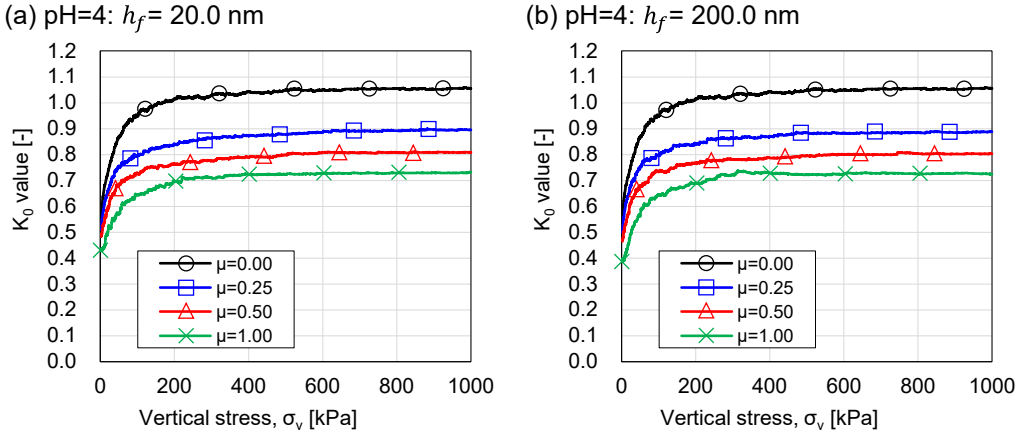

Fig. 4. K_0-σ_v' relationships for the pH=4 samples with different values of μ: (a) $h_f = 20$ nm, and (b) $h_f = 200$ nm.

Initially, the samples were isotropically compressed under p'=0.1 kPa (p' is a mean effective stress) to achieve an equilibrium state. As a result of the isotropic compression with p'=0.1 kPa, the pH=4 sample had a flocculated microfabric characterized by well-developed face-to-edge associations, while the pH=8 sample had a dispersed microfabric dominated by face-to-face associations. These microfabric formations agreed with SEM images [15]. After isotropic compression to p' =0.1 kPa, two series of the 1D compression simulations, the monotonic loading simulations and the unloading-reloading simulations, were performed. The monotonic loading simulations involved loading the samples until a vertical stress (σ_v') of 1000 kPa was reached, whereas the unloading-reloading simulations involved loading the samples up to $\sigma_v' = 200$ kPa, then unloading them to 10 kPa, followed by reloading them from 10 kPa to 1000 kPa. In the monotonic loading simulations, the influence of the interparticle friction parameters (specifically μ and h_f) on compression behaviour (such as K_0 value and compressibility) was investigated. On the other hand, the unloading-reloading simulations aimed to assess whether including interparticle friction might give a hysteretic response.

In these 1D simulations, four different μ values ($\mu = 0.0, 0.25, 0.5$ and 1.0) and two different h_f values ($h_f = 20$ and 200 nm) were used. It should be noted that these values were determined without clear physical evidence due to limited discussion on interparticle friction in particle-scale simulations, in particular CGMD simulations.

3.2 Monotonic loading simulations

3.2.1 Macroscopic behaviour

Fig. 3 shows the e-log(σ_v') relationships (e is the void ratio) for the pH=4 samples with different μ and h_f values. The influence of μ on the e - log(σ_v') relationships was pronounced while that of h_f was not remarkable. Regardless of the h_f value, the mechanical response became stiffer, and compressibility reduced as μ increased. Fig. 4 shows the K_0-σ_v' relationships for the pH=4 samples with different μ and h_f values. In all the pH=4 samples, K_0 increased monotonically with increasing σ_v'. The increase in K_0 became gradual from $\sigma_v' \approx 200$ kPa, converging to a constant value at $\sigma_v' \approx 500$ kPa, which means that K_0 has a stress-dependency. Considering the effect of μ on K_0, the samples which included interparticle friction (i.e. $\mu \neq 0.0$) obviously showed $K_0 < 1.0$ at $\sigma_v' = 1000$ kPa, while the frictionless sample (i.e. $\mu = 0.0$) showed $K_0 \approx 1.0$. These results indicated that K_0 decreased as μ increased. Comparing Figs. 4(a) and (b), it can be confirmed that h_f did not significantly affect the K_0-σ_v' relationships.

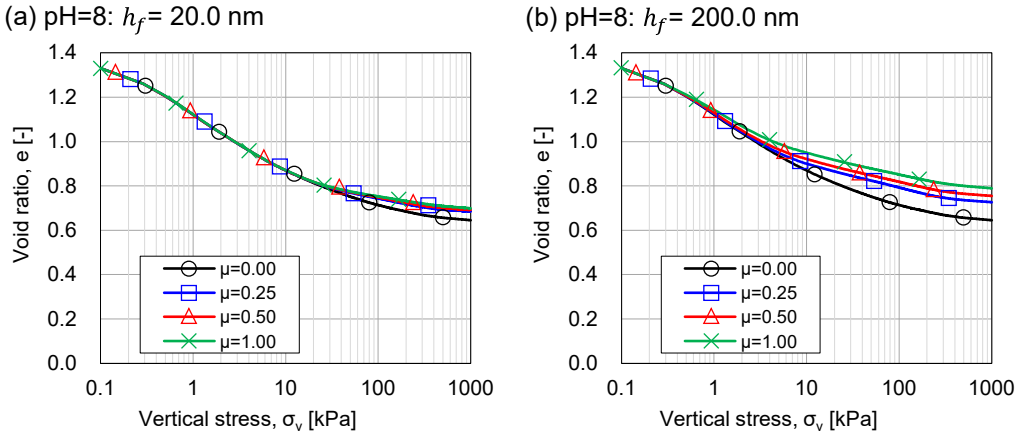

Fig. 5. e-log(σ_v') relationships for the pH=8 samples with different values of μ: (a) $h_f = 20$ nm, and (b) $h_f = 200$ nm.

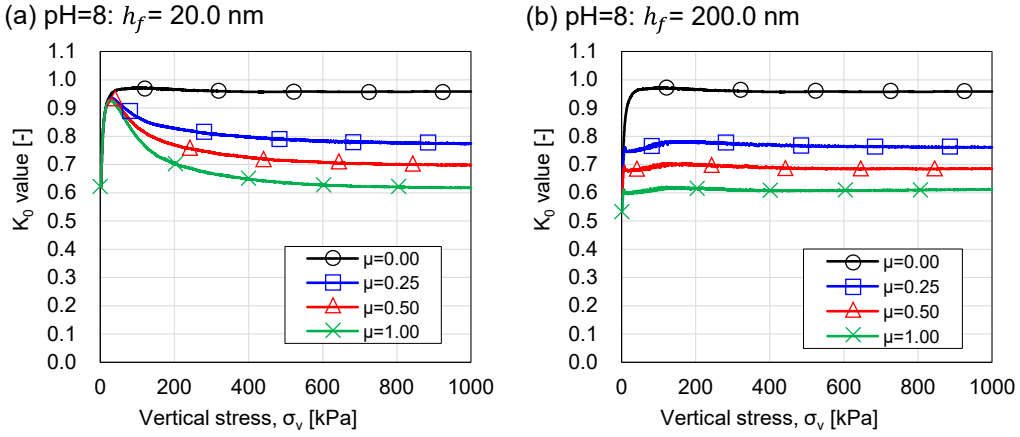

Fig. 6. K_0-σ_v' relationships for the pH=8 samples with different values of μ: (a) $h_f = 20$ nm, and (b) $h_f = 200$ nm.

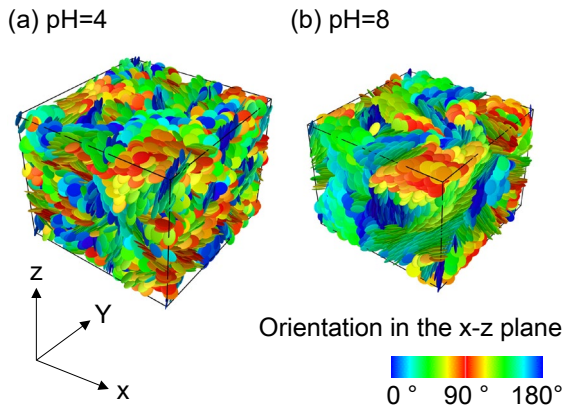

Fig. 7. Graphical rendering of virtual samples in the x-z plane: (a) pH4 sample with μ=1.0 and h_f=200 nm at σ_v'=1000 kPa, and (b) pH8 sample with μ=1.0 and h_f=200 nm at σ_v'=1000 kPa (particle orientation is the orientation of the minor principal axis of the ellipsoids projected onto the x-z plane).

Fig. 5 presents the e-log(σ_v') relationships for the pH=8 samples with different μ and h_f values. When h_f was 20 nm (see Fig. 5(a)), the influence of μ on the e-log(σ_v') relationships was relatively small and almost the same the e-log(σ_v') relationships were obtained. On the other hand, when h_f was 200 nm (see Fig. 5(b)), the mechanical response became stiffer as μ increased. Fig. 6 shows the K_0 - σ_v' relationships for the pH=8 samples with different μ and h_f values. These data indicate that h_f has a large impact on the K_0 - σ_v' relationships. When $h_f = 20$ nm, K_0 attained a peak (i.e. $K_0 = 0.9 \sim 1.0$) at $\sigma_v' \approx 50$ kPa. After that, K_0 of the frictionless sample remained, while in the other friction-introduced samples, K_0 reduced gradually and converged to a constant value at $\sigma_v' \approx 1000$ kPa. On the other hand, when $h_f = 200$ nm, K_0 was almost constant from the early stage of loading and was less dependent on σ_v'.

Atkinson et al. [16] showed that the experimental K_0 value of kaolinite was approximately 0.66. Hence, it was found that $\mu \approx 1.0$ is necessary to reproduce this value in CGMD simulations.

3.2.2 Particle-scale behaviour

The differences between the microfabrics seen in Fig. 7 are consistent with those observed in comparable SEM images [15].

To investigate more detailed information on the variation in microfabric during 1D compression simulations, the second-order fabric tensor (Φ_{ij}) defined by Eq. (1) was introduced [17,18].

$$\Phi_{ij} = \frac{1}{\mathrm{N}} \sum_{k=1}^{N} n_i^k n_j^k \tag{1}$$

where N is the total number of particles in the simulation box, n is the unit vector of the particle principal minor axis, i and j indicate the directional components ($i, j = x, y, z$). Φ_{zz}, which is one of the second-order fabric tensor components, presents the degree to which the particle minor axes are oriented in z-axis (vertical) direction (i.e. particles are horizontal).

Fig. 8(a) show the Φ_{zz}-log(σ_v') relationships for the pH=4 samples with different μ and $h_f = 200$ nm. In all pH=4 samples, Φ_{zz} increased as σ_v' increased, which means that the proportion of the horizontal particles increased. The frictionless sample showed a prominent increase in Φ_{zz} with σ_v', while in the other friction-introduced samples the increase in Φ_{zz} with σ_v' became smaller as μ increased. This trend implied that interparticle friction hinders particle rotation.

Fig. 8(b) show the Φ_{zz}-log(σ_v') relationships for the pH=8 samples with different μ and $h_f = 200$ nm. The increase in Φ_{zz} was not larger than that in the pH=4 samples (Fig. 8(a)), which suggested that the particles rotation was relatively prevented. The increase in Φ_{zz} with σ_v' became smaller as μ increased. This trend was consistent with that observed in the pH=4 samples, hence it can be also found that particle rotation was prevented by that interparticle friction.

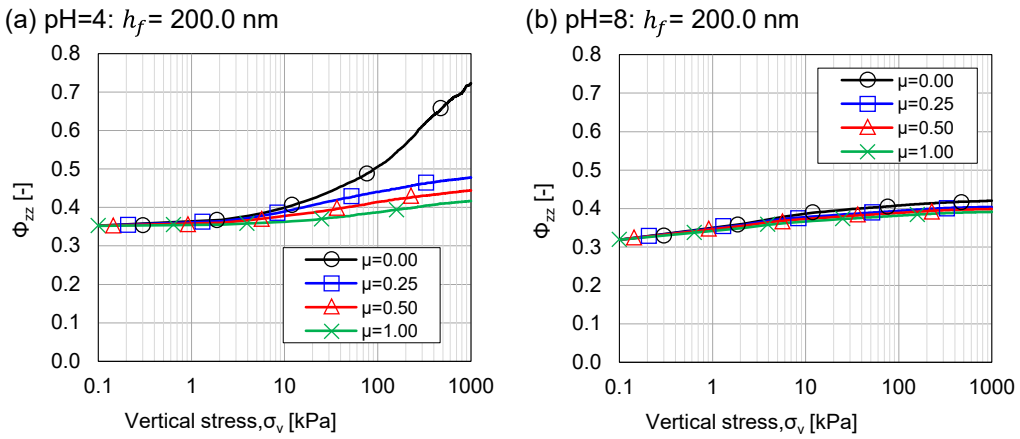

Fig. 8. The Φ_{zz}-log(σ_v') relationships (a) for the pH=4 samples with h_f=200 nm and different values of μ and (b) for the pH=8 samples with h_f=200 nm and different values of μ.

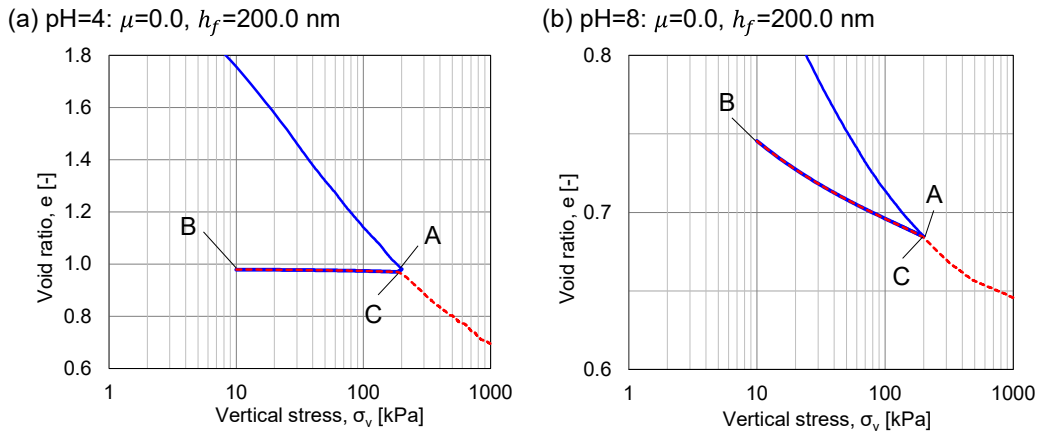

Fig. 9. The e-log(σ_v') relationships during unloading-reloading cycle: (a) for the frictionless pH=4 sample, and (b) for the frictionless pH=8 sample.

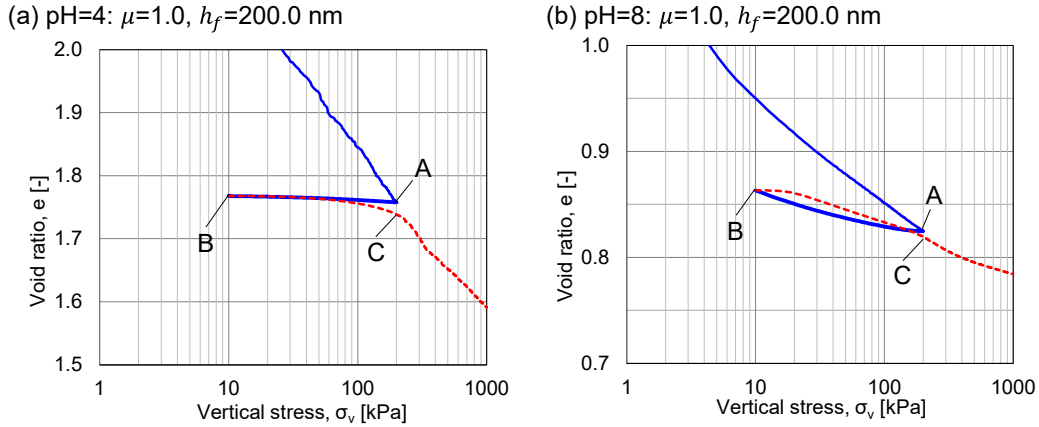

Fig. 10. The e-log(σ_v') relationships during unloading-reloading cycle: (a) for the pH=4 sample with $\mu = 1.0$ and $h_f = 200$ nm, and (b) for the pH=8 sample with $\mu = 1.0$ and $h_f = 200$ nm.

3.3 Unloading-reloading simulations

Fig. 9 shows the unloading-reloading behaviour in the e-log(σ_v') plane for the frictionless pH=4 and pH=8 samples. "A" in Fig. 9 indicates the start of unloading, "B" indicates the end of unloading / the start of reloading, and "C" indicates the end of reloading. For both friction less pH=4 and pH=8 samples, the unloading (A-B) curves and the reloading (B-C) curves completely overlapped. This behaviour did not obviously replicate physical reality.

Fig. 10 shows the unloading-reloading behaviour in the e-log(σ_v') plane for the pH=4 sand pH=8 samples with $\mu = 1.0$ and $h_f = 200$ nm. Introducing interparticle friction resulted in different paths for the unloading (A-B) curves and the reloading (B-C) curves. For the pH=4 sample, the unloading curve passed over the reloading curve. In this study, this type of hysteresis is referred as an "open hysteresis loop". On the other hand, for the pH=8 sample, the unloading curve passed below the reloading curve, which is referred as an "closed hysteresis loop". The closed hysteresis loop is closer to the unloading-reloading behaviour of kaolinite observed in laboratory tests.

The reason why the introduction of interparticle friction leads to reproduction of the hysteresis behaviour is that the potential energy between particles was transformed to heat and reduced by interparticle friction during the unloading-reloading cycle. This reduction in the potential energy caused the change in the interparticle distance and the particle rearrangement.

4 Conclusions

This study investigated the influence of the interparticle friction parameters (i.e. μ: coefficient of friction and h_f: cut-off length of interparticle friction) on 1D compression behaviour of normally consolidated kaolinite using coarse-grained molecular dynamics (CGMD) implementing the Coulomb friction model to describe the tangential (frictional) forces.

The results of the monotonic loading simulations showed that if interparticle friction was not considered K_0 became approximately 1.0, whereas if interparticle friction was simulated K_0 became less than 1.0. The data also showed that K_0 decreased as μ increased. The influence of h_f on the mechanical response during 1D compression was not remarkable in the pH=4 samples while that was more significant in the pH=8 samples.

This study also investigated the influence of interparticle friction on the unloading-reloading behaviour (i.e. hysteresis) during 1D compression. The simulation results identified that primary cause of the hysteresis observed on the e-log(σ_v') plane using the unloading-reloading cycle was the interparticle friction.

The results presented in this study have provided insight into the sensitivity of the macro-scale response observed in particle-scale simulations of clay to interparticle friction and highlight the need to develop reliable values for clay particle friction. The data presented in this study clearly demonstrate that fully atomistic molecular dynamics simulations are necessary to clarify the tangential component of clay interparticle interactions and determine optimal friction models and parameters.

References

1. D. Ebrahimi, A. J. Whittle, R. J. -M. Pellenq, Mesoscale properties of clay aggregates from potential of mean force representation of interactions between nanoplatelets. J. Chem. Physics. **140**, No. 15, 154309 (2014), https://doi.org/10.1063/1.4870932
2. B. Derjaguin, L. Landau, Theory of the stability of strongly charged lyophobic sols and of the adhesion of strongly charged particles in solutions of electrolytes. Prog. Surf. Sci. **43**, 30–59 (1941). https://doi.org/10.1016/0079-6816(93)90013-LA.
3. E. J. W. Verwey, J. T. G. Overbeek, Theory of the stability of lyophobic colloids. J. Phys. Colloid Chem. **51**, 631–636 (1948). https://doi.org/10.1021/j150453a001
4. X. Huang, K. J. Hanley, C. O'Sullivan, C. Y. Kwok, Exploring the influence of interparticle friction on critical state behaviour using DEM. Int. J. Numer. Anal. Methods Geomech. **38** (2014). https://doi.org/10.1002/nag.2259
5. A. A. Peña, A. Lizcano, F. Alonso-Marroquin, H. J. Herrmann, Biaxial test simulations using a packing of polygonal particles. Int. J. Numer. Anal. Methods Geomech. **32** (2008). https://doi.org/10.1002/nag.618
6. Z. X. Yang, J. Yang, L. Z. Wang, On the influence of inter-particle friction and dilatancy in granular materials: A numerical analysis. Granul. Matter **14** (2012). https://doi.org/10.1007/s10035-012-0348-x
7. S. Bandera, T. Morimoto, C. O'Sullivan, P. Tangney, S. Angioletti-Uberti, Effects of the absence of friction in coarse-grained molecular dynamics simulations of clay. Int. J. Geomech. **24**, 04024213 (2024). https://doi.org/10.1061/IJGNAI.GMENG-9235
8. Y. Nakamichi, C. O'Sullivan, P. Tangney, S. Angioletti-Uberti, Modelling anisotropic surface charge of kaolinite particles depending on pore water pH. Comput. Geotech. **173**, 106505 (2024). https://doi.org/10.1016/j.compgeo.2024.106505
9. Y. Nakamichi, C. O'Sullivan, P. Tangney, S. Angioletti-Uberti, S. Bandera, Exploring the linkage between mechanical behaviour and particle-scale interaction of kaolinite. Géotechnique, 1–18 (2025). https://doi.org/10.1680/jgeot.23.00193
10. Y. Nakamichi, C. O'Sullivan, P. Tangney, S. Angioletti-Uberti, Effects of interparticle friction on the one-dimensional compression behaviour of clay. Int. J. Geomech. (2025), in press.
11. J. G. Gay, B. J. Berne, Modification of the overlap potential to mimic a linear site-site potential. J. Chem. Phys. **74** (1981). https://doi.org/10.1063/1.441483
12. Y. H. Wang, W. K. Siu, Structure characteristics and mechanical properties of kaolinite soils. I. Surface charges and structural characterizations. Can. Geotech. J. **43**, 587–600 (2006a). https://doi.org/10.1139/T06-026
13. Y. H. Wang, W. K. Siu, Structure characteristics and mechanical properties of kaolinite soils. II. Effects of structure on mechanical properties. Can. Geotech. J. **43**, 601–617 (2006b). https://doi.org/10.1139/T06-027
14. V. Gupta, M. A. Hampton, J. R. Stokes, A. V. Nguyen, J. D. Miller, Particle interactions in kaolinite suspensions and corresponding aggregate structures. J. Colloid Interface Sci. **359**, 95–103 (2011). https://doi.org/10.1016/j.jcis.2011.03.043
15. M. Pedrotti, A. Tarantino, An experimental investigation into the micromechanics of non-active clays. Géotechnique **68**, 666–683 (2018). https://doi.org/10.1680/jgeot.16.P.245
16. J. H. Atkinson, D. Richardson, P. J. Robinson, Compression and extension of K_0 normally consolidated kaolin clay. J. Geotech. Eng. **113**, 1468–1482 (1987). https://doi.org/10.1061/(ASCE)0733-9410(1987)113:12(1468)
17. M. Satake, Constitution of mechanics of granular materials through the graph theory. In: Proc. US–Japan Seminar on Continuum Mechanics and Statistical Approaches in the Mechanics of Granular Materials, Sendai, pp. 203–215 (1978).
18. M. Satake, Fabric tensor in granular materials. In: IUTAM Conference on Deformation and Failure of Granular Materials (1982), pp. 63–68.